Polymer 50 (2009) 296–304

Contents lists available at ScienceDirect

Polymer

journal homepage: www.elsevier.com/locate/polymer

Rate-dependent large deformation behavior of PC/ABS

Qin-Zhi Fang [a,b,*], T.J. Wang [a], H.G. Beom [b], H.P. Zhao [a]

[a] MOE Key Laboratory for the Strength and Vibration, Department of Engineering Mechanics, Xi'an Jiaotong University, Xi'an 710049, China
[b] Department of Mechanical Engineering, Inha University, Incheon 420-751, Republic of Korea

ARTICLE INFO

Article history:
Received 2 May 2008
Received in revised form
29 September 2008
Accepted 23 October 2008
Available online 6 November 2008

Keywords:
Digital image correlation method
Large deformation
Constitutive model

ABSTRACT

Rate-dependent large deformation behavior of the alloy of polycarbonate and acrylonitrile–butadiene–styrene (PC/ABS) is experimentally investigated over a crosshead speed range of 1–3000 mm/min. Three-dimensional non-contact digital image correlation (DIC) method is used to measure the large deformation of polymer specimens. Numerical simulation of geometry effect on the necking process of specimens is done for the specimen with two section sizes. It is found that the width contracts less than the thickness due to its larger size than the thickness for specimens with rectangular sections, and the relations between two lateral contraction ratios and engineering strains are geometry dependent, but independent of loading speeds. The influence of strain rates on local volume ratios of PC/ABS is also discussed. Based on the experimental results, a simple phenomenological constitutive model with six parameters is proposed for the glassy polymer, in which the effect of strain rate and its variation during constant crosshead speed loading tests is considered, and can be used in constant true strain rate or constant principal stretch rate loading condition.

1. Introduction

Polymers have been widely used in a number of structures such as automobiles, aircraft, spacecraft, pressure vessels and pipes. Modeling and predicting of the deformation and failure behavior of polymers become very important for the structures made of polymers. However, investigations of the deformation and failure of polymers are still in its infancy. This is mainly because polymers have much more complicated mechanisms of deformation and failure compared to metals. Large inelastic deformation involving strain softening and/or hardening [1–3] is one of the characteristics of glassy polymers such as PC, PMMA, PC/ABS blends, which makes the glassy polymers highly prone to the localization of plastic deformation.

It is well known that the constitutive model of material is essential for modeling and predicting of the deformation and failure of structures and materials. However, how to establish a reasonable constitutive model to describe the large inelastic deformation behavior of glassy polymers is still an open problem, even though extensive works have been devoted to this field and several theoretical models have been proposed in the past decades. The well-known theoretical constitutive model to describe the large inelastic deformation of glassy polymers was proposed by Boyce et al. [4–6] on the basis of the kinematics of molecular chains and later modified by Wu and van der Giessen [7,8] and Basu and van der Giessen [9]. Drozdov and Christiansen [10] proposed a constitutive model for nonlinear time-dependent response of isotactic polypropylene by dividing the network with passive mesoregions (with affine junctions) and active mesodomains (where junctions can slide with respect to their reference positions with various rates) two separate parts. Theoretical models have great assistance to the understanding of the micro- and macroscopic mechanisms of the deformation and fracture of polymers.

Phenomenological constitutive models are generally convenient for engineering applications. In the past decades, several useful phenomenological models have also been proposed to describe the large inelastic deformation of polymers. G'Sell and Jonas [11] proposed a constitutive equation used for describing the flow curves of polymers. Using the Maxwell elements, Bardenhagen et al. [12] proposed a three-dimensional viscoplastic constitutive model of polymers. More recently, Duan et al. [13] developed a more general phenomenological constitutive model for glassy and semicrystalline polymers, which includes eight material parameters and is applied to some polymers. Considering the effect of internal damage, Fahmi et al. [14] developed a constitutive model for rubber-modified polymer, in which the strain softening, strain hardening, sensitivity of strain rate and evolution of void are included. Based on their experimental results, Fang et al. [15] proposed a three-stage phenomenological model for PC/ABS alloy, in which the strain rate effect is not included.

* Corresponding author. MOE Key Laboratory for the Strength and Vibration, Department of Engineering Mechanics, Xi'an Jiaotong University, Xi'an 710049, China. Tel./fax: +86 29 82665168.
E-mail address: fangqz@mail.xjtu.edu.cn (Q.-Z. Fang).

0032-3861/$ – see front matter © 2008 Elsevier Ltd. All rights reserved.
doi:10.1016/j.polymer.2008.10.042

It is well known that the reliable experimental results are the basis of establishing accurate constitutive models of polymers, which depend on the accurate measurement of the large deformation of polymers. Usually, necking in polymeric specimens occurs at relatively small strain, which results in the inhomogeneous deformation of polymers. In this case, the conventional extensometers are generally questionable or useless. So, how to evaluate the large inhomogeneous deformation of polymers is another open problem and alternate method is required.

In the past two decades, several methods have been developed to measure the large deformation of polymers. Spaced grid lines method was used by several researchers [16–19], with which the instantaneous distances between the lines were measured and then the true stress and strain curves of polymers were obtained. Another efficient way was proposed by G'Sell et al. [20], in which a special video-controlled tensile testing system was developed to measure in situ the stress and strain curves and the volume changes of PET and HIPS polymers. Using the method given in [20], Bai and Wang [21] studied the plastic damage mechanisms of PP/PA6/POE blends under cyclic tension. However, these methods can only show the average strain between points in a small distance apart. Recently, digital image correlation (DIC) analysis method is successfully employed to measure the large deformation of polymers and appears its advantages over the previous ones. Based on the DIC method and using a non-intrusive digital speckle laser extensometer, Laraba-Abbes et al. [22] developed a coarse–fine search method to measure the large deformation of rubber-like materials and then obtained the two-dimensional in-plane displacement fields and local strain of carbon black filled natural rubber. Parsons et al. [23] developed a data reduction scheme to determine the local strain history at individual points on the specimens with DIC method. Using this method, they studied the large inhomogeneous deformation behavior of net PC and successfully obtained the full-field strain contours and volumetric strain. Berfield et al. [24] applied the DIC technique across multiple length scales through the generation of a suitable speckle pattern at each size scale. For microscale measurements, a random speckle pattern of paint was created with a fine point airbrush. Nanoscale displacement resolution was achieved with a speckle pattern formed by solution deposition of fluorescent silica nanoparticales. Fang et al. [2,25] developed a new method to measure accurately the large tensile deformation behavior of polymers through the simultaneous measurement of three-dimensional deformation of the specimen on the basis of DIC method, in which the deferent deformation behaviors in three directions of specimens can be measured without any assumption.

Rate-dependent large-strain mechanical properties of polymers are of great importance in engineering and scientific research. Briscoe and Hutchings [26] studied the flow stress of high density polyethylene at low strain rates by using a commercial testing machine and high strain rate with a projectile method. Briscoe and Nosker [27] studied the influence of interface friction on the compressive yield properties of a high density polyethylene with a Split Hopkinson pressure bar (SHPB) equipment. Yi et al. [28] studied the large rate-dependent stress–strain compression behavior of polyurea and polyurethanes by quasi-static compression testing and SHPB testing. Roland et al. [29] studied the high strain rate mechanical behavior of polyurea in uniaxial tension over a range of strain rates from 0.06 to 573 s^{-1} on a drop weight test instrument. Jordan et al. [30] studied the compressive properties of polytetrafluoroethylene across strain rate from 10^{-3} to 10^{5} s^{-1} with commercial test machine and SHPB equipment. Due to the difficulty of strain measurement, they only take average strain rate or reference strain rate as the effective strain rate to describe the rate-dependent deformation by ignoring the variation of strain rate caused by the inhomogeneous deformation of polymers after yielding. However, the effect of the strain rate variation cannot be ignored in some loading case, if the strain rate effect on the deformation behavior of polymers is strong enough. The development of the DIC measurement technique makes it possible to measure the variation of local strains. It is therefore possible to investigate the effect of the variation of local strain rates on the deformation performance of polymers.

Here, the rate-dependent large deformation behaviors of PC/ABS are experimentally investigated over a crosshead speed range of 1 to 3000 mm/min. The three-dimensional non-contact digital image correlation (DIC) method proposed by the present authors [2] is modified and used to measure accurately the large deformation of polymers, in which a new method is included to calculate the strain fields with the measured displacement fields. High speed cameras are used to record the deformation of specimens. The variation of local volume deformation ratio and strain rate is discussed. The geometry effect on the necking deformation is discussed with numerical simulation. The true stress–strain curves of PC/ABS tested with different loading speeds are obtained. Based on the experimental results, a phenomenological constitutive model is proposed, in which the variation of strain rates due to the inhomogeneous deformation behaviors of polymer is considered.

2. Test and results

2.1. Materials and specimens

The material used here is PC/ABS with blend ratio of PC to ABS being 70/30. The average molecular weight of PC is 30,000 g/mol. The minor phase ABS with pellet sizes of 0.2–0.5 μm is uniformly distributed among the continuum phase PC. It is inject molded into dumb-bell tensile specimen as shown in Fig. 1. The injection temperature is 300–320 °C, and the holding pressure is 60–80 MPa.

2.2. Displacement measurement

Tensile tests are performed following ASTM D-638 standard at room temperature (about 16° C) air environment by using a Zwick Z005 universal tensile machine. The three-dimensional DIC method proposed [2] is used to measure the surface displacements of specimens, in which two digital cameras or two high speed cameras are used simultaneously to record the deformation images of the two surfaces of specimens during tensile tests at lower or higher speed, respectively, as shown in Fig. 2. The detailed description of the method and its verification can be found in literature [2]. Random speckle pattern is sprayed on the specimen surfaces with three different inks (black, blue and red) (For interpretation of the references to color in this figure legend, the reader is referred to the web version of this article.) as shown in Fig. 3. The coordinates system is also shown in Figs. 2 and 3. The specimens are loaded to failure with constant crosshead speeds in the tensile

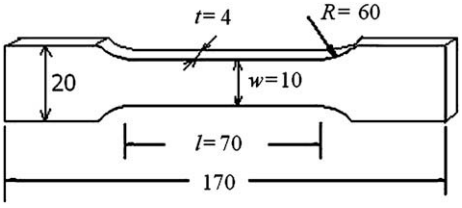

Fig. 1. Geometry and dimensions of the tensile specimen.

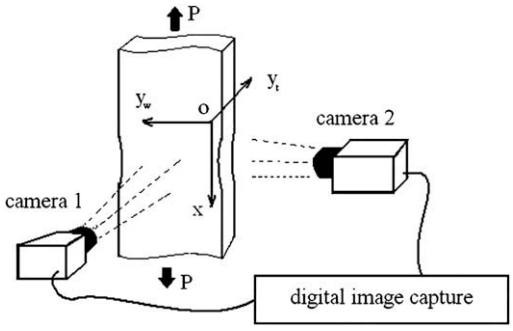

Fig. 2. Set-up of the deformation measurement system.

test. The crosshead speeds used in the test for different specimens are 1, 5, 25, 625 and 3000 mm/min. Images are taken at a speed as high as 1 picture per second for the tensile tests with crosshead speeds of 1, 5 and 25 mm/min. For the tensile tests with crosshead speeds of 625 and 3000 mm/min, images are taken with two high-speed cameras at a speed of 60 pictures per second. Efforts are made to start loading and image capturing simultaneously to keep synchronization of the image capturing and loading. Moreover, we can correlate the loading data with each image according to the load vs. time data and image vs. time data by the fracture points for each specimen. To ensure necking locates within the gage region, the width near the center of the specimen is reduced by about 0.1 mm with fine grit sand papers.

Fig. 3 shows several deformation images of the width surface at different tension stages for a PC/ABS specimen tested at a cross-head speed of 25 mm/min. On the specimen surface image taken at the very beginning of each test, coordinates and a square region to be measured are chosen as that shown in Fig. 3(a). Then, the displacement fields at each following tensile stage can be obtained.

As an example, Fig. 4 shows the axial and lateral displacement fields at the tensile stage of 1.133 s from the beginning, which corresponds to a maximum engineering tensile strain of about 0.67 at the middle section of the necking region, for a specimen tested at a crosshead speed of 3000 mm/min. (x, y) denotes the pixel coordinates of points in the un-deformed image for the specimen. The $u(x,y)$ and $v(x,y)$ are the overall displacements at point (x,y) in x and y directions, respectively. It is seen that the displacement fields $u(x,y)$ and $v(x,y)$ vary significantly in the necking deformation stage. The shearing deformation is nearly symmetric in the necking region.

2.3. Calculation of strain fields

The sketch of the strain calculation method is also illustrated in Fig. 4(a). If we intend to calculate the strains at point (x_i,y_i), then

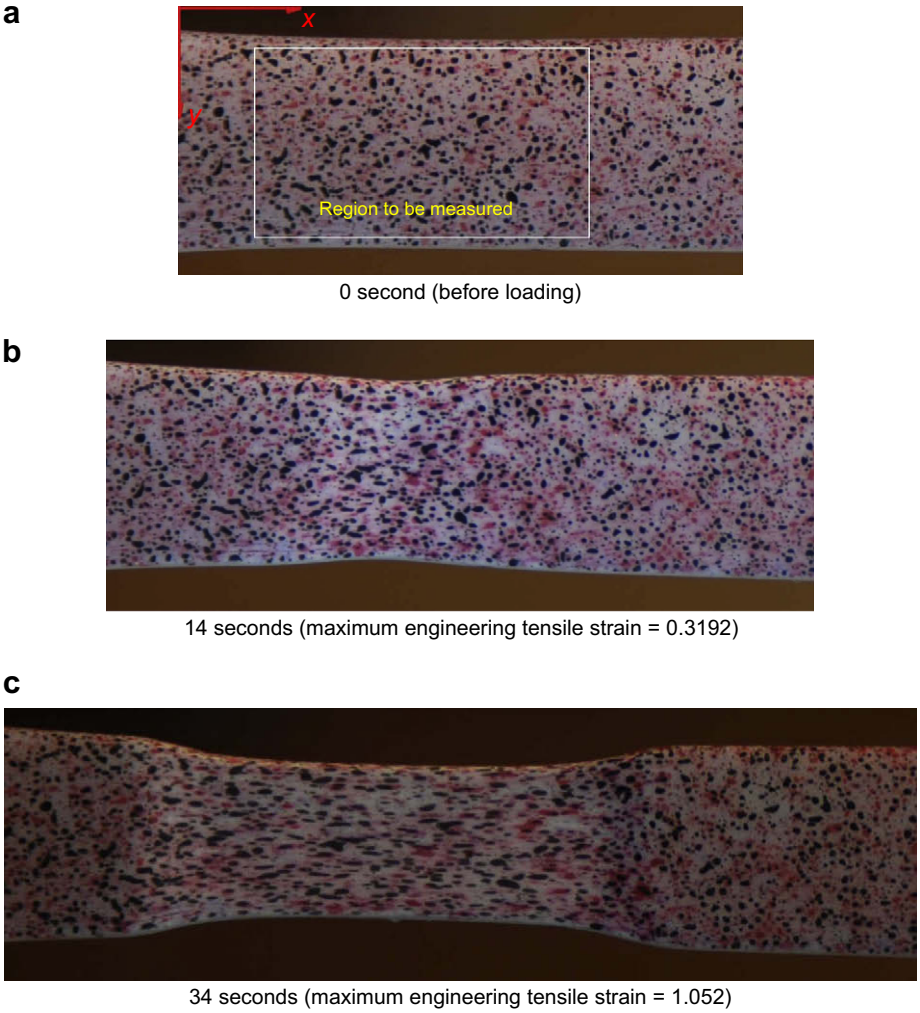

Fig. 3. Deformation images of a specimen tested at crosshead speed of 25 mm/min.

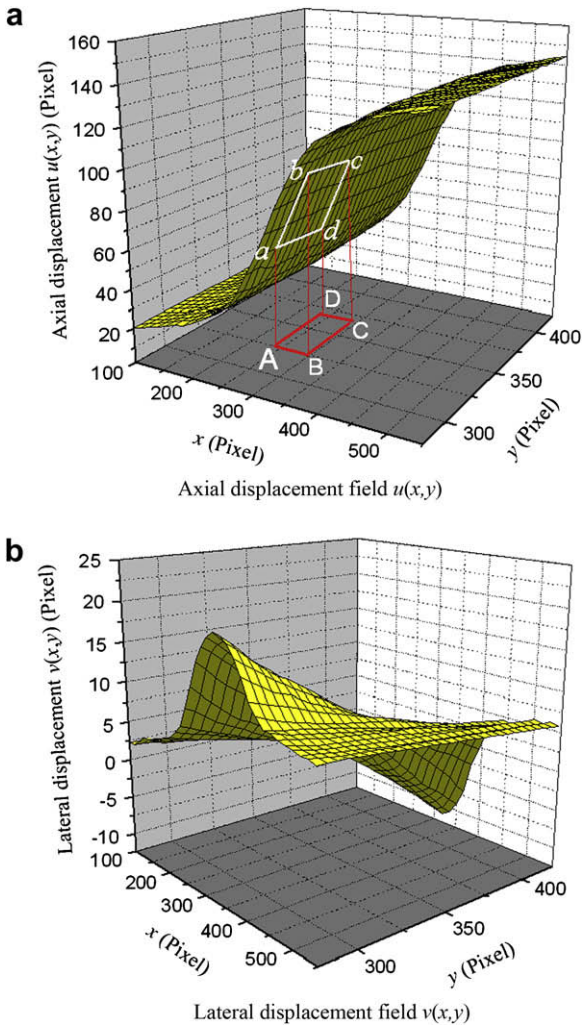

Fig. 4. Surface displacement fields at time stage 1.133 s for a specimen tested with a cross speed of 3000 mm/min.

a square subset ABCD ($x_i - k_s \le x \le x_i + k_s, y_i - l_s \le y \le y_i + l_s$) around point ($x_i$,$y_i$) is selected, where the values of k_s and l_s are chosen according to the variations of displacement fields. If the displacement fields change smoothly in x (or y) direction, larger values of k_s (or l_s) are chosen; otherwise, smaller values of k_s (or l_s) are taken. Fitting the axial or lateral displacement fields over the subset ABCD, we then obtain the displacement fields $u(x,y)$ or $v(x,y)$ on the subset. The engineering strains can be calculated as follows, although larger deformation is considered here.

$$\varepsilon_{ex} = \frac{\partial u}{\partial x} \tag{1}$$

$$\varepsilon_{ey} = \frac{\partial v}{\partial y} \tag{2}$$

$$\gamma_{xy} = \frac{\partial u}{\partial y} + \frac{\partial v}{\partial x} \tag{3}$$

Fig. 5 shows the engineering strain fields calculated from the displacement fields shown in Fig. 4. It is clear that the axial and lateral strains are nearly constant along lines perpendicular to the axial direction (i.e. at fixed x position). It is learned from Fig. 5, at the middle of the necking region where the maximum tensile engineering strain and minimum section area is obtained, the shear strains γ_{xy} are vanishing although there are shear strains appeared

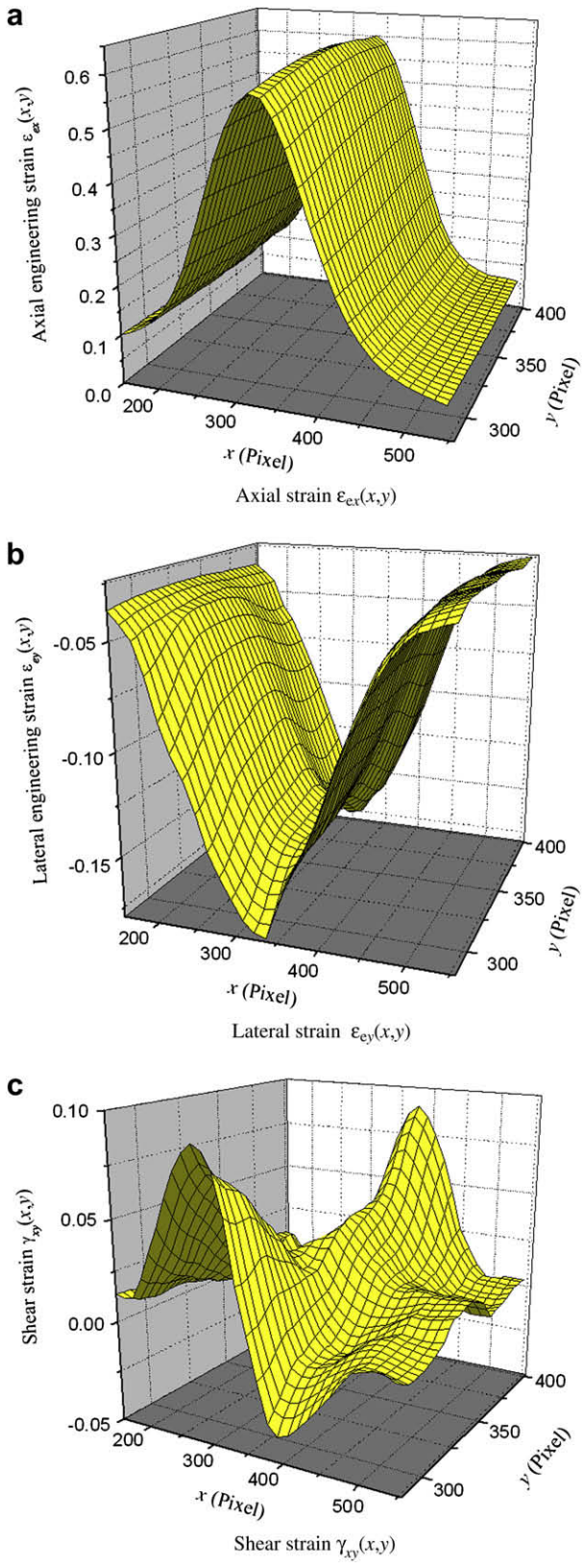

Fig. 5. Strain fields calculated from the displacement fields shown in Fig. 4.

in the necking region apart from the middle section area. That means the engineering strains in x and y directions on the middle section are principal engineering strains. It has been deducted that the engineering principal strains ε_{e1} and ε_{e2} can be obtained for small as well as large strains with the following transformation.

$$\varepsilon_{e1} = (\varepsilon_{ex} + \varepsilon_{ey})/2 + \sqrt{(\varepsilon_{ex} - \varepsilon_{ey})^2 + \gamma_{xy}^2}/2$$
$$\varepsilon_{e2} = (\varepsilon_{ex} + \varepsilon_{ey})/2 - \sqrt{(\varepsilon_{ex} - \varepsilon_{ey})^2 + \gamma_{xy}^2}/2 \quad (4)$$

The angle of the direction of the principle strain with-axis α can be given with

$$\tan 2\alpha = -\gamma_{xy}/(\varepsilon_{ex} - \varepsilon_{ey}) \quad (5)$$

It is seen from Fig. 5(c) that the shear strains at the middle section of the necking region are vanishing. At the regions apart from the middle section of the necking region, shear strains γ_{xy} are much lower than the $(\varepsilon_{ex}-\varepsilon_{ey})$, therefore its effect on the engineering principal strain fields is small according to Eq. (4).

The average axial and lateral engineering principal strains of the specimen for any fixed x position are calculated and given in Fig. 6. Here, the symbols ε_e and ε_{eyw} denote the maximum average axial principal strain and the minimum lateral principal strains obtained from the displacement fields on the width surface of the specimen, respectively. The symbol ε_{eyt} denotes the minimum average lateral principal strains obtained on the thickness surface of the specimen.

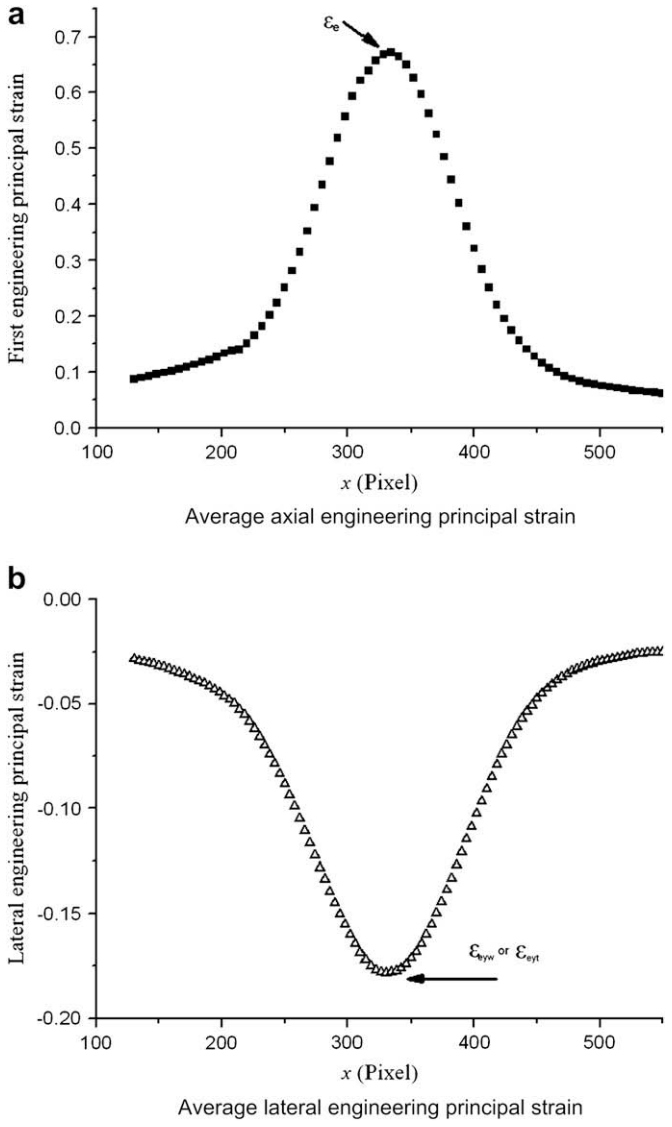

Fig. 6. Variations of the average strains along tensile direction obtained with the strain fields shown in Fig. 5.

For the large strains, the average axial true strain ε can be calculated [2,20] as:

$$\varepsilon = \ln(1 + \varepsilon_e) = \ln \lambda \quad (6)$$

where the parameter $\lambda = 1 + \varepsilon_e$ is the local principal stretch.

The local principal stretch on the thickness surface can also be obtained with the maximum average axial principal engineering strains on thickness surface.

The true strains given with Eq. (6) can be used to represent the maximum axial true strains of the specimen at the tension stage, and the λ on the width surface is used to represent the principal stretch of the specimen.

2.4. Necking deformation

It is seen from Fig. 6(a) that ε_{eyw} and ε_{eyt} are the minimum average lateral engineering strains of the specimen. The ratio of the minimum width w to the initial width w_0 of the specimen can be calculated as:

$$\frac{w}{w_0} = 1 + \varepsilon_{eyw} \quad (7)$$

Similarly, we obtain the ratio of the minimum thickness t to the initial width t_0 of the specimen,

$$\frac{t}{t_0} = 1 + \varepsilon_{eyt} \quad (8)$$

Fig. 7 shows the necking ratio $(w/w_0)/\lambda$ or $(t/t_0)/\lambda$ vs. tensile engineering strain $(\lambda - 1)$ for specimens with different loading rate. It is found that the necking ratios in width direction are significantly different from that in thickness direction for all the specimens tested at different crosshead speeds. It can also be found that the necking ratios in width direction or in thickness direction are not affected by the loading speeds. This means each of the necking ratios vs. tensile engineering strains at minimum necking section are independent of the loading speeds.

The difference of the necking ratios in two lateral directions can be caused by the different sizes and/or anisotropy deformation properties in width and thickness directions. The anisotropy deformation cannot be simulated reasonably without the anisotropy properties of the polymer. Here, the numerical calculation of

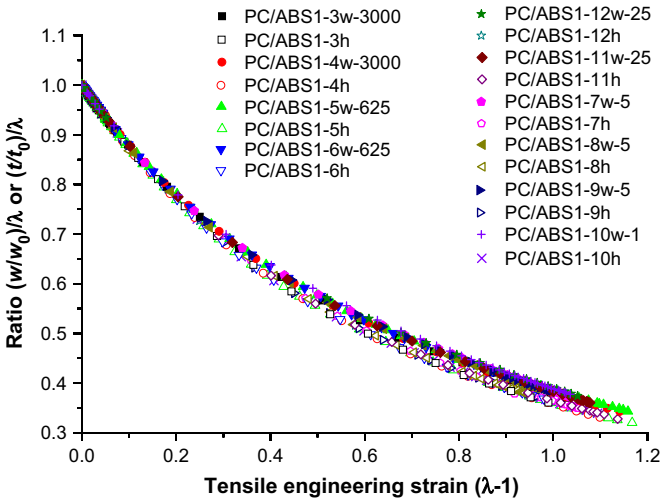

Fig. 7. Necking ratio vs. tensile engineering strain for specimens tested at different strain rates. PC/ABS1-x represents specimen number; the letters w and h after the specimen number represent width and thickness, respectively. The number behind the letter w is the crosshead speed in a unit of mm/min.

the necking process is done with ABAQUS FEM code to simulate only the geometry effect on necking deformation process by assuming the material being isotropic. The true stress–strain curve obtained in the experiment for specimens tested at crosshead speed of 1 mm/min is separated into elastic and plastic parts as needed by the ABAQUS FEM code, and used as the material model in the computation. Two specimen geometries are used here to show the geometry effect on the necking behaviors of specimens. One of the specimen geometry is the same as that shown in Fig. 1 with a section size of 10×4 mm, and another is the same except the section size is changed as 10×10 mm. Fig. 8 shows the necking ratios obtained with the numerical simulation. The definition of the symbols and the calculation of each parameter are exactly same as that used in the experiment. It is found that the necking ratios in two lateral directions are significantly different for the specimen with a section size of 10×4 mm just as that given in the experiment (Fig. 7), while the necking ratios in two lateral directions are same for the specimen with a section size of 10×10 mm. This means geometry is one of the main reasons to cause the difference of the necking ratios in two lateral directions. Therefore, it can be concluded that the relationships between the necking ratios and tensile strain are dependent on the geometry.

It is well known that dilatational deformation is an important phenomenon for polymers. G'Sell et al. [20] and Parsons et al. [23] have measured the volume variations of different polymers through different methods. They gave the volume deformation ratio by the summation of three principal strain components, in which they took the two lateral strains as same by assuming the strain tensor transversally isotropic. However, because only the surface strains of the specimens can be measured, it is difficult to give the volume deformation ratios accurately. In this study, the following formula is used to calculate the volume ratio at the minimum section of specimens.

$$\frac{V}{V_0} = (1+\varepsilon_e)\left(\frac{w}{w_0}\right)\left(\frac{t}{t_0}\right) = (1+\varepsilon_e)(1+\varepsilon_{eyw})(1+\varepsilon_{eyt}) \tag{9}$$

In obtaining this formula, it is assumed that the minimum specimen sections remain rectangular during the whole tensile deformation process. As shown in Fig. 5(a), the tensile strains at the minimum section are higher in the middle than that near the edges of the specimen during necking deformation process. The deformation is concentrated in a smaller distance in the middle part than that near the edges, as shown in Fig. 3(b). The lateral contraction strains here are also inhomogeneous, as shown in Fig. 5(b). The specimen contracts more near the edges of the specimen due to the less constraint. In the stable necking deformation stage, the minimum section can be recognized as rectangular section reasonably, and therefore Eq. (9) gives a reasonable volume deformation ratio in the stable tensile stages. Fig. 9 shows the volume ratio variations calculated with Eq. (9) for PC/ABS specimens tested at different loading rate. It is seen that the ratio V/V_0 increases with the increase of true axial strain for PC/ABS, which is in agreement with [20,23], and then decreases gradually. It is also found that the maximum volume ratio seems to decrease and the position at which the maximum volume ratio reached seems to increase to a higher true strain with the increasing of the loading rates, although there is some scatter of the experimental data in Fig. 9.

2.5. True strain rate

It is known that the strain rate does not keep constant during the tensile process with the constant crosshead speed loading policy due to the inhomogeneous deformation behavior of polymers [2]. Therefore, it is necessary to consider the effect of the strain rate variation, while trying to give a constitutive formulation of the true stress–strain of polymer under the basis of the experimental results.

The local principal stretch rate is given as:

$$\dot{\lambda} = \frac{d\lambda}{dt} = \frac{d\varepsilon_e}{dt} \tag{10}$$

The true strain rate is given as:

$$\dot{\varepsilon} = \frac{d\varepsilon}{dt} \tag{11}$$

Therefore, according to Eq. (6)

$$\dot{\lambda} = e^{\varepsilon}\dot{\varepsilon} \tag{12a}$$

$$\dot{\varepsilon} = \frac{\dot{\lambda}}{\lambda} \tag{12b}$$

The true strain rates for each specimen can be obtained with the strain fields obtained in the experiment. Fig. 10(a) and (b) show the true strain rate variation of specimens during tensile test with crosshead speeds of 3000 and 5 mm/min, respectively. It is found that the strain rate has significant variation during the tensile loading process, and the maximum strain rates are

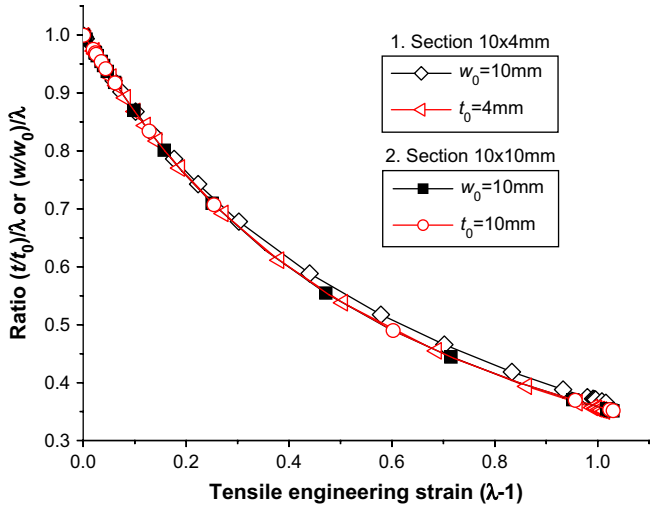

Fig. 8. Numerical simulation of necking ratios for specimens with different section sizes.

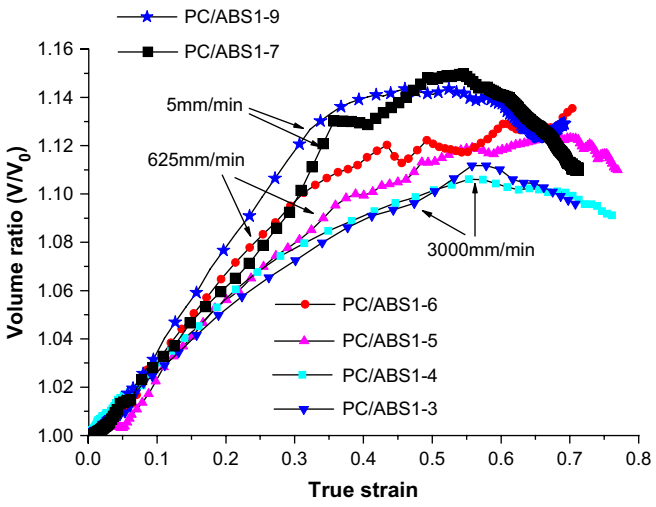

Fig. 9. The volume ratio at the minimum section of specimens tested at different crosshead speeds.

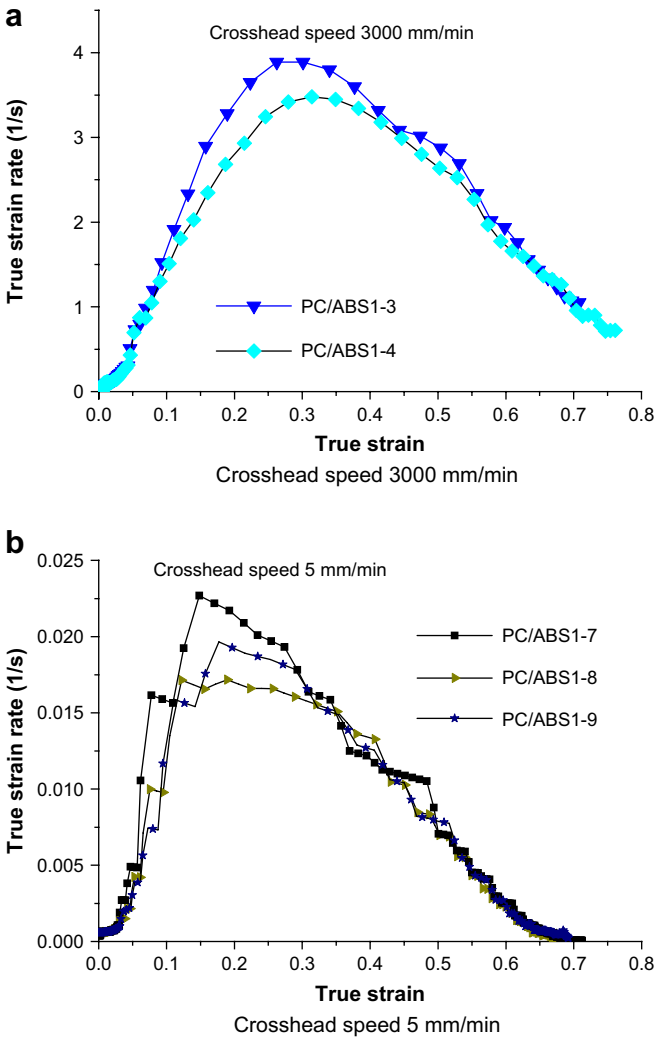

Fig. 10. Strain rate for different specimens.

different for different specimens even with same crosshead loading speed due to the scatters of the geometry and material behaviors. This must be considered in the formulation of constitutive model.

2.6. True stress–strain curve

The true stress is calculated as

$$\sigma_{\text{true}} = \frac{P}{wt} = \frac{P}{w_0 t_0} \Big/ \left(\frac{w}{w_0}\frac{t}{t_0}\right) \tag{13}$$

where P is the load applied to specimens. The true stress and strain curves of the specimens tested at different crosshead speeds are shown in Fig. 11. Fig. 11(a)–(e) shows the experimental stress–strain curves obtained for the specimens tested at crosshead speeds of 3000, 625, 25, 5 and 1 mm/min, respectively. The deformation of PC/ABS alloy can be separated roughly into elastic, yielding and orientation hardening stages. Unlike the stress–strain curves obtained in literatures [20,23], there is almost no strain softening in these stress–strain curves just after yielding. This is due to the consideration of the different deformation properties in two lateral directions, as shown in Fig. 7. In what follows, a simple and efficient phenomenological constitutive model is developed to describe the deformation behavior of PC/ABS alloy on the basis of the measured stress and strain curves shown in Fig. 11.

3. Phenomenological constitutive model

Based on the true stress–strain curves shown in Fig. 11 and the previous phenomenological constitutive models [13], the following function can be used to describe the first two (elastic and yielding) deformation stages of the polymers:

$$\sigma = k[1 - \exp(-\beta\varepsilon)]^{\xi} \tag{14}$$

where k, β and ξ are material parameters.

k is related with the yield stress which depends on the elastic strain rate, which is equal to the initial principal stretch rate $\dot{\lambda}_0$ in the study. The initial principal stretch rate$\dot{\lambda}_0$ is given with the crosshead speed c divided with the specimen gage length l ($l = 70$ mm as shown in Fig. 1)

$$\dot{\lambda}_0 = \frac{c}{l} = \frac{c}{70} \tag{15}$$

where c is the crosshead speeds which are taken as 50, 10.416, 0.416, 0.0833 and 0.0167 mm/s, respectively. The unit of $\dot{\lambda}_0$ is 1/s. Because only elastic homogeneous deformation occurred within the gage length before yielding, therefore, $\dot{\lambda}_0$ reflects the initial elastic principal stretch rate of the specimens. After yielding, the overall strain rate $\dot{\varepsilon}$ (or the overall principal stretch rate$\dot{\lambda}$), which reflects mainly the strain rate of inelastic deformation after yielding, increases rapidly in the inhomogeneous necking deformation stage, as shown in Fig. 10. This has a great effect on the stress–strain curves. According to the experimental results, it is found that the effect can be introduced by a modification of the parameter k, which is given as:

$$k = \left(\sigma_0 + \mu\sqrt{\dot{\lambda}/\dot{\lambda}^*}\right) \tag{16a}$$

$$\sigma_0 = A + \eta \ln\left(\dot{\lambda}_0/\dot{\lambda}^*\right) \tag{16b}$$

where A and η are material constants. $\dot{\lambda}^* = 1.0$ (1/s) is the reference principal stretch rate.

It is found that the parameter β has a great effect on the initial stiffness of the stress–strain curves, which also depend on the initial elastic principal stretch rate $\dot{\lambda}_0$ with the form of the following formula:

$$\beta = B + \kappa\sqrt{\dot{\lambda}_0/\dot{\lambda}^*} \tag{17}$$

where B and κ are material constants.

Because ξ has only a weak relation with the loading conditions, 2 is assigned to the parameter ξ to reduce a variable in the constitutive model.

Generally, the distribution of polymer chain length can be described with log normal distribution function. Therefore, it is reasonable to describe the stress and strain responses of polymers after yielding by using the following function [15],

$$\sigma = C + \sigma_{01}\exp\left[-\frac{1}{2}\left(\frac{\varepsilon - \varepsilon_{\text{m}}}{s}\right)^2\right] \tag{18}$$

where C, σ_{01}, ε_{m} and s are material parameters.

Combining Eqs. (14), (16–18), and let $\sigma_{01} = \sigma_0$, a simple phenomenological constitutive model is obtained as,

$$\sigma = \left(\sigma_0 + \mu\sqrt{\dot{\lambda}/\dot{\lambda}^*}\right)[1 - \exp(-\beta\varepsilon)]^2 + \sigma_0\exp\left[-\frac{1}{2}\left(\frac{\varepsilon - \varepsilon_{\text{m}}}{s}\right)^2\right] \tag{19a}$$

$$\sigma_0 = A + \eta \ln\left(\dot{\lambda}_0/\dot{\lambda}^*\right) \tag{19b}$$

$$\beta = B + \kappa\sqrt{\dot{\lambda}_0/\dot{\lambda}^*} \tag{19c}$$

which includes six parameters to be identified according to the experimental results.

By fitting to the experimental results given in the study, the following phenomenological constitutive formula is obtained for PC/ABS in term of principal stretch rate as Eq. (20).

$$\begin{aligned}\sigma = & \left[63.60 + 1.10\ln\left(\frac{\dot{\lambda}_0}{\dot{\lambda}^*}\right)\right. \\ & \left. + 2.0\sqrt{\frac{\dot{\lambda}}{\dot{\lambda}^*}}\right]\left\{1 - \exp\left[-\left(117.37 - 65.91\sqrt{\frac{\dot{\lambda}_0}{\dot{\lambda}^*}}\right)\varepsilon\right]\right\}^2 \\ & + \left[63.60 + 1.10\ln\left(\frac{\dot{\lambda}_0}{\dot{\lambda}^*}\right)\right]\exp\left[-\frac{1}{2}\left(\frac{\varepsilon - 1.09}{0.30}\right)^2\right]\end{aligned} \tag{20}$$

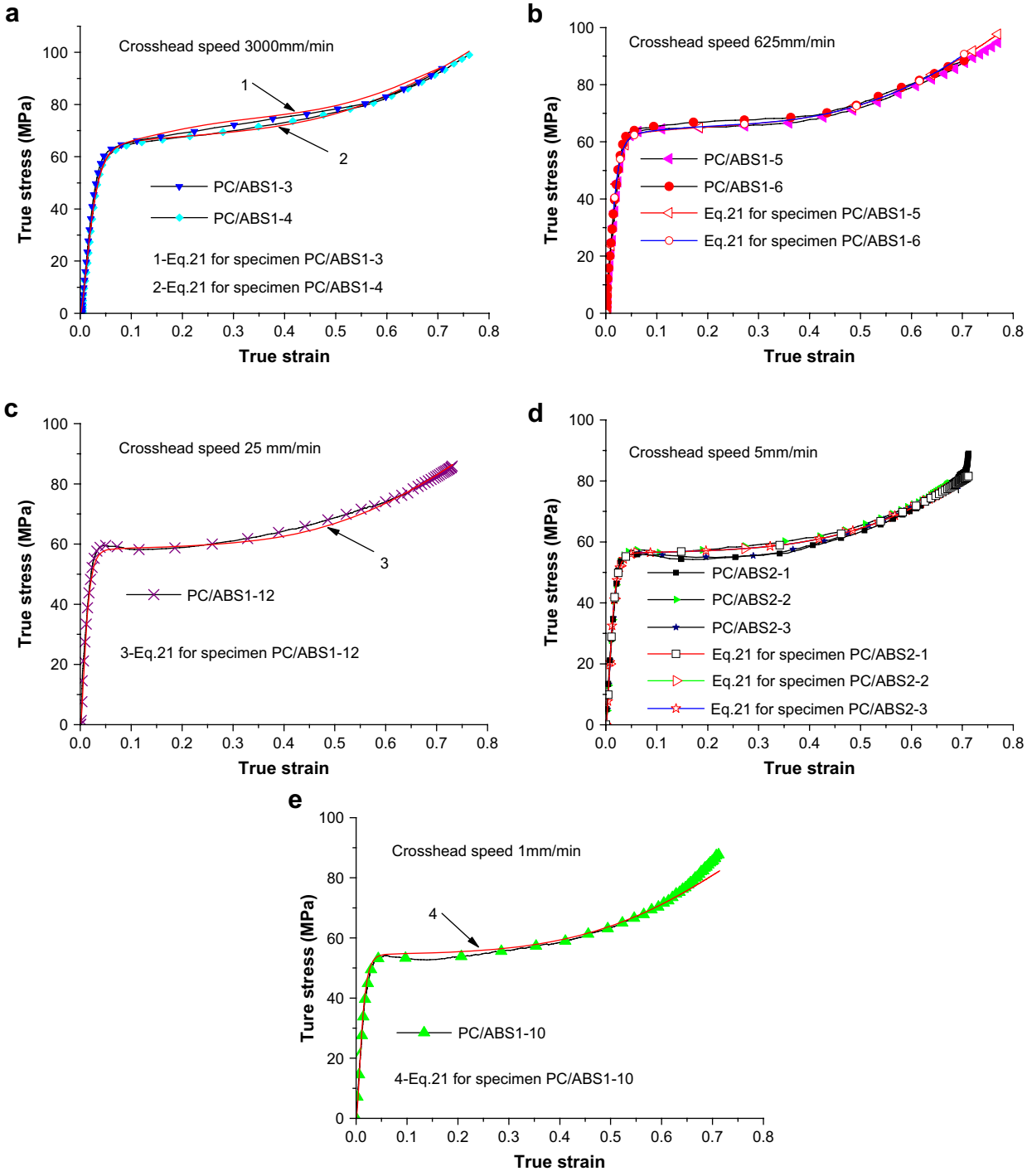

Fig. 11. True stress–strain curves for PC/ABS alloy tested with different crosshead speed.

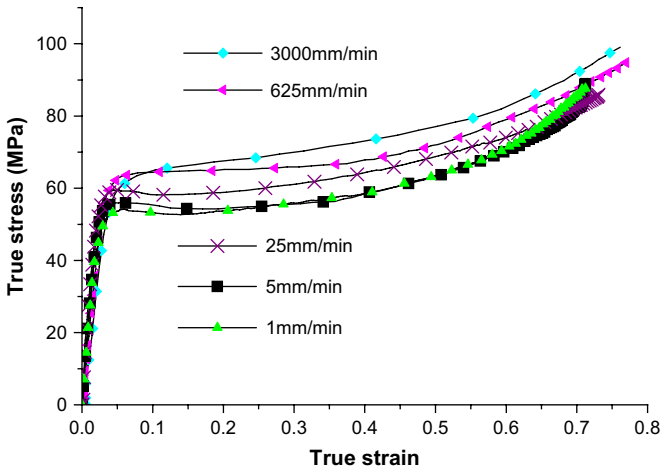

Fig. 12. The effect of the crosshead speed (strain rate) on the true stress–strain curves.

Substitute Eq. 12(a) in Eq. (19), then the phenomenological constitutive formula in terms of true strain rate is obtained for PC/ABS according to the experimental results.

$$\sigma = \left(63.60 + 1.10\ln\left(\frac{\dot{\lambda}_0}{\dot{\lambda}^*}\right) + 2.0\exp\left(\frac{\varepsilon}{2}\right)\sqrt{\frac{\dot{\varepsilon}}{\dot{\lambda}^*}}\right) \times \left\{1 - \exp\left[-\left(117.37 - 65.91\sqrt{\frac{\dot{\lambda}_0}{\dot{\lambda}^*}}\right)\varepsilon\right]\right\}^2 + \left[63.60 + 1.10\ln\left(\frac{\dot{\lambda}_0}{\dot{\lambda}^*}\right)\right]\exp\left[-\frac{1}{2}\left(\frac{\varepsilon - 1.09}{0.30}\right)^2\right] \quad (21)$$

Fig. 11 (a)–(e) shows also the lines predicted with the phenomenological constitutive model (Eq. (20) or (21)) for specimens tested at crosshead speeds of 3000, 625, 25, 5 and 1 mm/min, respectively. It is found that the phenomenological constitutive model fits the experimental results well.

Fig. 11(a) shows the stress–strain curves given with the experiment results as well as that given by Eq. (20) or (21) while taking into the consideration of the strain rate variation of the two specimens tested at a crosshead speed of 3000 mm/min. It is found that the phenomenological constitutive model fits the experimental results well, and can discriminate the different experimental results due to the difference of the true strain rates in the necking deformation stage, as shown in Fig. 10(a).

Fig. 11(d) shows the stress–strain curves given with the experimental results as well as that predicted with Eq. (20) or (21) for the three specimens tested at a crosshead speed of 5 mm/min. It is found that the effects of the true strain rates in the necking deformation stage on the stress–strain curves are small compared to the larger effects of the strain rate on stress–strain curves given in Fig. 11(a). This phenomenon can also be explained from Eq. (20) or (21). According to the phenomenological constitutive model, the true stress is influenced by the square root of principal stretch rate $\dot{\lambda}$. The effect is larger for higher value of the principal stretch rate $\dot{\lambda}$ or true strain rate $\dot{\varepsilon}$. Therefore, it can be concluded that the effect of the variation of the strain rate due to the inhomogeneous necking deformation can be ignored for a lower strain rate, due to the relative small value of the square root of principal stretch rate $\dot{\lambda}$. But its effect cannot be ignored for a higher strain rate. As we know, it is hard to conduct a constant true strain rate test for polymers due to its inhomogeneous deformation behaviors after yielding. With the method given in the research, we can predict the true stress–strain behaviors of constant principal stretch rate (in which $\dot{\lambda} = \dot{\lambda}_0$) or constant true strain rate simply by letting $\dot{\lambda} = \dot{\lambda}_0$ or $\dot{\varepsilon} = \dot{\lambda}/\lambda =$ constant, respectively.

The effect of the elastic strain rate, which is given in term of $\dot{\lambda}_0$ in the model, cannot be ignored for both low and high strain rate. Fig. 12 shows parts of the experimental stress–strain curves of PC/ABS tested at different crosshead speeds. It is shown that the strain rate has significant effects on the true stress–strain curves of PC/ABS.

4. Conclusions

A modified three-dimensional non-contact digital image correlation (DIC) method is proposed and used in this paper to measure accurately the large deformation of polymers, from which one can obtain the displacement fields and the strain fields. The true stress–strain curves tested with a range of crosshead speeds (from 1 to 3000 mm/min) are experimentally obtained for PC/ABS. It is found that the relationships between the necking ratio and the tensile strain are dependent on the geometry, and independent on the loading rate. Based on the experimental results, a simple phenomenological constitutive model with six parameters is proposed for the glassy polymer, in which the effect of strain rate variation during a constant crosshead speed loading test is considered, and can be used in constant true strain rate or constant principal stretch rate loading condition. The variation of the strain rate in the necking deformation stage can be ignored for lower strain rates as shown in Fig. 11(d), but cannot be ignored for higher strain rate as shown in Fig. 11(a). The effect of the elastic strain rate, which is given in term of $\dot{\lambda}_0$, cannot be ignored for low and high rates of strain.

Acknowledgements

This work is supported by NSFC (10472087 and 10672129). The polymer material was provided by Nanjing Julong Engineering Plastics Corporation.

References

[1] Lai J, van der Giessen E. Mechanics of Materials 1997;25:183–97.
[2] Fang Q-Z, Wang TJ, Li HM. Polymer 2006;47:5174–81.
[3] Hoy RS, Robbins MO. Journal of Polymer Science, Part B: Polymer Physics 2006;44(24):3487–500.
[4] Boyce MC, Parks DM, Argon AS. Mechanics of Materials 1988;7(1):15–25.
[5] Boyce MC, Weber GG, Parks DM. Journal of the Mechanics and Physics of Solids 1989;37(5):647–57.
[6] Boyce MC, Arruda EM. Polymer Engineering and Science 1990;30:1288–98.
[7] Wu PD, van der Giessen E. Mechanics Research Communication 1992;19(5):427–37.
[8] Wu PD, van der Giessen E. Journal of the Mechanics and Physics of Solids 1993;41:427–56.
[9] Basu S, van der Giessen E. International Journal of Plasticity 2002;18:1395–423.
[10] Drozdov AD, Christiansen J. Journal of Rheology 2003;47:595–618.
[11] G'Sell C, Jonas JJ. Journal of Materials Science 1979;14:583–91.
[12] Bardenhagen SG, Stout MG, Gray GT. Mechanics of Materials 1997;25:235–53.
[13] Duan Y, Saigal A, Greif R, Zimmerman NA. Polymer Engineering and Science 2001;41(8):1322–8.
[14] Fahmi Z, Moussa NA, Krzysztof W, Jean-Michel G. European Journal of Mechanics A/Solids 2005;24:169–82.
[15] Fang QZ, Wang TJ, Li HM. Key Engineering Materials 2006;326–328:127–30.
[16] Buisson G, Ravichandar K. Polymer 1989;31:2071–6.
[17] G'Sell C, Hiver JM, Dahoun A, Souahi A. Journal of Materials Sciences 1992;27:5031–9.
[18] Haynes AR, Coates PD. Journal of Materials Science 1996;31:1843–55.
[19] Meyer RW, Pruitt LA. Polymer 2001;42:5293–306.
[20] G'Sell C, Hiver JM, Dahoun A. International Journal of Solids and Structures 2002;39:3857–72.
[21] Bai SL, Wang M. Polymer 2003;44:6537–47.
[22] Laraba-Abbes F, Ienny Piques R. Polymer 2003;44:3883–91.
[23] Parsons E, Boyce MC, Parks DM. Polymer 2004;45:2665–84.
[24] Berfield TA, Patel JK, Shimmin RG, Braun PV, Lambros J, Sottos NR. Experimental Mechanics 2007;47:51–62.
[25] Fang QZ, Wang TJ, Beom BG, Li HM. Polymer Degradation and Stability 2008;93(8):1422–32.
[26] Briscoe BJ, Hutchings IM. Polymer 1976;17:1099–102.
[27] Briscoe BJ, Nosker RW. Wear 1984;95:241–62.
[28] Yi J, Boyce MC, Lee GF, Balizer E. Polymer 2006;47:319–29.
[29] Roland CM, Twigg JN, Vu Y, Mott PH. Polymer 2007;48:574–8.
[30] Jordan JL, Siviour CR, Foley JR, Brown EN. Polymer 2007;48:4184–95.